And., Intl.,J., Appl Sci., Eng., Tech, Vol 05, No 02, July 2025
e-ISSN: 2797-0442

Effects of Angle of Attack (AoA), Aspect Ratio, and Leading-Edge Curvature on Supersonic Fin Performance

M. Hasbi Ash Shiddieqy, Andoko Andoko*
Department of Mechanical and Industrial Engineering, Universitas Negeri Malang, Indonesia,
*Coressponding author, e-mail: andoko.ft@um.ac.id

Abstract— The aerodynamic optimization of fin-stabilized rockets operating under supersonic conditions remains a key challenge in aerospace engineering. Existing studies often isolate geometric factors, lacking a comprehensive analysis of their combined effects. This study employs a full-factorial design of experiments (DoE) coupled with computational fluid dynamics (CFD) simulations using the k-ω SST turbulence model to evaluate the effects of angle of attack (AoA), fin aspect ratio, and leading-edge radius of curvature at Mach 3. Quantitative results show that a moderate AoA of 5°–10° yields the highest lift-to-drag ratios, increasing from 0.0007 at 0° to 4.82 at 10°. Lower aspect ratios (0.3) produced up to 38% higher lift compared to higher values, while a 20 mm increase in leading-edge curvature enhanced lift by 8% and reduced drag by 0.6%. These findings emphasize the importance of integrated geometric optimization to control shock structures, minimize separation, and improve high-speed aerodynamic performance. This framework provides a scientific basis for optimizing fin design in supersonic vehicles, offering practical guidance for aerospace engineers developing efficient, high-performance configurations.

Keywords: Supersonic flow, Fin geometry, Computational fluid dynamics, Lift-to-drag ratio, Design of experiments.

This article *is licensed under the CC–BY-SA license.*

1. Introduction

The design of fin-stabilized rockets operating under supersonic flow regimes involves numerous aerodynamic challenges that significantly influence stability, control, and propulsion efficiency. Among these challenges, the balance between aerodynamic drag and flight stability remains a key concern. Fins, while essential for passive stabilization, inherently contribute to increased aerodynamic drag, thereby reducing overall flight performance [1]. Furthermore, innovations such as fin canting or moveable configurations have emerged as viable methods to mitigate drag while enhancing trajectory control and aerodynamic efficiency across various phases of flight [2]. These design adjustments also facilitate enhanced manoeuvrability, enabling rockets to respond dynamically to changing flight conditions. Optimizing fin-stabilized rockets is vital for applications such as military guided munitions, space launch vehicles, and sounding rockets. Enhanced aerodynamic efficiency translates to improved range, stability, and control authority, particularly in high-speed missions through varying atmospheric conditions.

The complexity of supersonic flow environments introduces additional challenges, including shock wave interactions and flow separation. These phenomena are particularly influenced by fin geometry, including leading-edge curvature and angle of attack. At supersonic velocities, flow separation caused by adverse pressure gradients can undermine lift generation and amplify drag. Moreover, considerations for thrust vector control (TVC) and aeroelastic responses must be addressed. Finless designs can utilize advanced TVC for directional control, but they often lack the inherent stability provided by fins [3]. Meanwhile, aeroelastic vibrations resulting from aerodynamic loads may compromise structural integrity, necessitating careful fin design for high-speed applications [4]. Addressing these

Received: June 5, 2025, Revised: July 17, 2025, Accepted: July 20, 2025
https://doi.org/10.25077/aijaset.v5i02.243

interconnected aerodynamic and structural challenges is crucial for ensuring mission success. In light of these aerodynamic complexities, a central problem persists in optimizing fin geometry to improve aerodynamic efficiency without compromising stability or structural resilience. Traditional fin design paradigms often struggle to provide optimal lift-to-drag ratios across the operational flight envelope. The need to control shock wave formation, reduce separation zones, and sustain favorable pressure gradients is compounded by the limited capacity of simplified design approaches to address such multidimensional performance criteria. The dynamic interplay between fin geometry and high-speed aerodynamic phenomena necessitates a more integrated, data-driven design methodology.

Computational fluid dynamics (CFD) has emerged as a principal methodology to overcome these limitations [5]. By offering precise visualization and analysis of flow behavior, CFD enables comprehensive assessments of how fin parameters such as angle of attack, aspect ratio, and leading-edge curvature influence aerodynamic performance. [6] illustrated the utility of CFD in predicting and optimizing lift and drag coefficients, while [7] highlighted the applicability of the k-ω SST model in turbulence modeling for supersonic flows. Thus, CFD serves as a robust platform to systematically investigate and refine fin configurations. These tools also allow for iterative design optimization that would be impractical through physical testing alone [8]. Advanced turbulence modeling strategies have further enhanced the fidelity of CFD simulations in aerospace applications. The k-ω Shear Stress Transport (SST) model remains a widely accepted approach for predicting boundary layer behavior under compressible, high-speed conditions. This model combines the advantages of both k-ε and k-ω formulations, allowing for accurate predictions near wall boundaries while adapting to free-stream conditions. Despite some over-prediction tendencies noted by [7], its integration with compressibility corrections renders it a suitable choice for the present context. Detached Eddy Simulation (DES) offers an alternative approach that combines Reynolds-Averaged Navier-Stokes (RANS) and Large Eddy Simulation (LES) capabilities. [9] emphasized DES's utility in resolving turbulent structures around complex geometries without incurring the high computational costs of full DNS or LES. These models facilitate a more detailed examination of shock-boundary layer interactions and other critical flow phenomena relevant to fin performance. Moreover, recent research underscores the importance of validating CFD outcomes with experimental data. Studies by [10] demonstrate how empirical comparisons strengthen the credibility of computational models. Furthermore, research by [11] has shown how evolving CFD techniques have enhanced accuracy in simulating transonic and supersonic aerodynamic behavior, supporting their application in performance prediction and design optimization. Validation efforts serve not only to confirm simulation accuracy but also to identify areas where model improvements are necessary for reliable prediction.

The geometric characteristics of fins—notably angle of attack (AoA), aspect ratio, and leading-edge curvature—are known to exert significant influence on aerodynamic forces. [12] demonstrated the critical role of AoA in dictating lift and drag coefficients, particularly in relation to flow separation. [13] and [14] further explored how variations in aspect ratio and curvature shape affect pressure gradients, vortex stability, and maneuverability. Despite these insights, the literature often treats these geometric factors in isolation or limited pairwise combinations. [15] and [16] have highlighted the need for integrated studies encompassing multiple geometric variables. Weaver and [17] pointed out deficiencies in turbulence model validation, particularly for high-speed applications where compressibility plays a critical role. [18] also identified challenges related to modeling assumptions and boundary condition uncertainties.

This study aims to investigate the aerodynamic effects of three critical fin parameters—AoA, aspect ratio, and leading-edge radius of curvature—on the performance of a fin-stabilized rocket operating at Mach 3. The primary objective is to assess how variations in these parameters influence the aerodynamic coefficients of lift and drag, with particular attention to their interactive effects. The novelty of this research lies in its application of a full-factorial DoE approach, which enables simultaneous evaluation of multiple geometric variables across defined levels. Unlike most existing studies that examine one or two parameters independently, this method facilitates a comprehensive analysis of their combined influence, leading to a deeper understanding of aerodynamic behavior under supersonic conditions. The

investigation utilizes high-fidelity CFD simulations based on the k-ω SST turbulence model, with all parameter variations embedded into a 3D finned rocket configuration. However, to date, no existing study has examined the combined influence of AoA, aspect ratio, and leading-edge curvature within a full-factorial CFD framework, leaving a significant gap in current aerodynamic optimization strategies. In addition to its scientific relevance, optimizing fin-stabilized rockets has practical importance for applications such as military projectiles, satellite launch vehicles, and sounding rockets, where aerodynamic efficiency directly impacts range, stability, and control. While this study provides detailed steady-state aerodynamic insights, it does not consider unsteady effects, aeroelastic deformation, or thermal-structural interactions, which are recommended for future work.

2. Method

2.1 Model Design

The rocket model utilized in this study consists of three main components: the nosecone, the body, and the fins. The primary focus of this research is on analyzing the airflow behavior around the fins under different angles of attack (0°, 5°, and 10°) and at a freestream Mach number of 3. The geometric configuration of the rocket is characterized by several key dimensions, including the length of the nosecone (L1), the length of the body (L2), the fin position relative to the body (L3), and the diameter of the rocket (D). The fin geometry is defined using parameters such as the aspect ratio (a/b), fin thickness (t), radius of curvature (R), swept angles (x1, x2), fin span (a), and chord length (b).

The rocket has a diameter of 60 mm. To avoid overlapping and ensure optimal spacing, a maximum fin span of approximately 31.4 mm is adopted, accommodating a total of six fins evenly distributed around the rocket body. The complete geometric specifications are illustrated in Figure. 1, which depicts the overall rocket geometry, and Figure. 2, which presents the configuration of angles of attack. Additionally, the detailed dimensional values for all rocket segments and fin parameters are summarized in Table. 1. These dimensions form the baseline for computational modeling and parametric variation within the scope of the aerodynamic simulations.

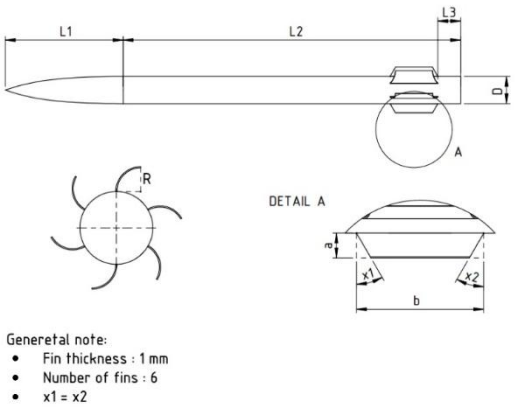


Figure 1. Rocket Geometry

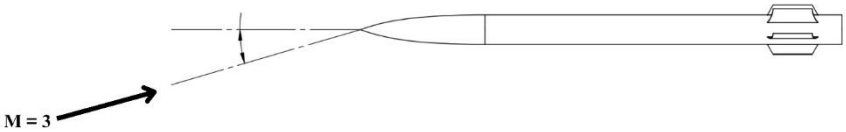


Figure 2. AoA

The final 3D geometry was then exported to the meshing software, where it was discretized using unstructured mesh elements. Care was taken to refine the mesh around critical flow regions, particularly near the fin leading edges and tip regions, to capture the complex shock-wave and boundary-

layer interactions. The meshed model, depicted in Figure. 3 and Figure. 4, was subsequently imported into the simulation environment for preprocessing and numerical solving.

Table 1. Geometry Detail

Segment	Value
nosecone (L1)	258.4 mm
body (L2)	740 mm
fin position (L3)	50 mm
diameter rocket (D)	60 mm
ratio a/b	0.3, 0.5, 0.8
radius of curvature (R)	(20, 30, 40) mm
swept angles (x1, x2)	30^o
fin span (a)	31.4
chord length (b)	(104.67, 62.8, 39.25) mm



Figure 3. 3D Model Rocket

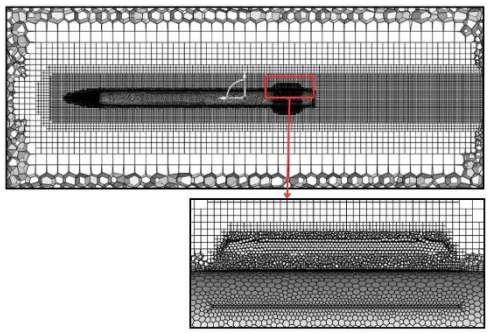


Figure 4. Meshing

2.2 Numerical Set-up

The simulations were carried out using a CFD solver, with physical modeling configured to replicate high-speed compressible flow conditions. The energy equation was enabled to capture thermal effects, and the flow regime was modeled using the k-ω Shear Stress Transport (SST) turbulence model, which is known for its robustness in resolving boundary layers under high-speed conditions. Air was modeled as an ideal gas with the following properties: specific heat capacity (Cp) of 1006.43 J/kg·K, thermal conductivity of 0.0242 W/m·K, and molecular weight of 28.966 kg/kmol. Viscosity followed the Sutherland law. Boundary conditions were assigned as follows: the farfield was set to pressure farfield with Mach 3 and a reference pressure of 101325 Pa at 300 K, while the rocket surface was treated as a no-slip wall. Simulation initialization was conducted using hybrid initialization. The calculation was run for 500 iterations or until convergence criteria were met. Convergence was assessed by monitoring the residuals and ensuring minimal changes in drag and lift coefficients across iterations. The relevant variables extracted from the simulation include the Mach number, Coefficient of Drag (Cd), and Coefficient of Lift (Cl).

2.3 Paramaters

The key output parameters measured in this study were the aerodynamic coefficients: Cd and Cl. These coefficients provide quantitative insights into the aerodynamic efficiency and stability of the rocket configuration under varying flow and geometrical conditions. Additionally, pressure and temperature distributions around the fin and body surfaces were extracted from the simulation. These results were visualized using contour plots, facilitating the identification of flow separation zones, shock

formations, and thermal gradients. The pressure and temperature fields were examined along three positions on the fin chord: the front, middle, and back sections, shown in Figure. 5.

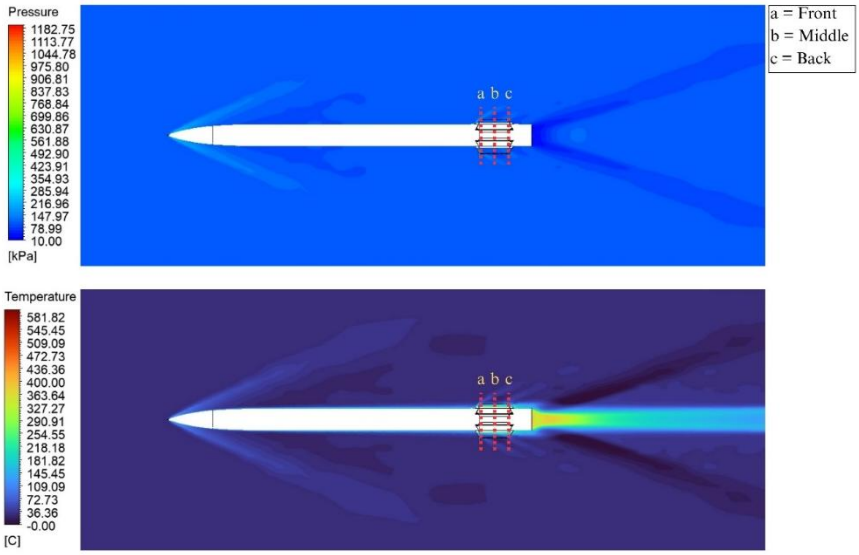


Figure 5. Pressure and Temperature Contours of The Rocket

3. Result and Discussion

3.1 Influence of Angle of Attack (AoA)

The simulation results demonstrate a clear and progressive trend in the aerodynamic coefficients as the AoA increases under supersonic conditions at Mach 3. As shown in Figure. 6 and Figure. 7, the Cd and Cl increase with rising AoA from 0° to 10°. At an AoA of 0°, the flow remains largely attached, yielding minimal drag and negligible lift, as indicated by Cl values approaching zero. At AoA = 5°, Cl experiences a notable increase to approximately 0.00087, while Cd exhibits a marginal rise to about 0.00058. This increase is primarily due to the realignment of the flow and enhanced pressure differential across the fin surfaces. At AoA = 10°, Cl rises sharply to approximately 0.0030, with Cd increasing moderately to about 0.00062, reflecting the formation of strong vortices and early onset of shock-induced separation, corroborating trends observed in Table. 2 and Figure. 9. Further insights from Figure. 8 show intensified pressure zones and thermal gradients near the leading edge and fin tips at 5° and 10° AoA, indicating the development of asymmetrical flow fields and complex shock-wave interactions and vortex structures.

The increased thermal load and asymmetry at higher AoA align with (Chainok et al., 2021) and (Coschignano et al., 2019), highlighting boundary-layer interactions and shock-induced separation. Aerodynamic trends are consistent with [19] and [20] who reported steady lift coefficient increases with AoA due to improved flow attachment and surface area, as well as [21], [22] emphasizing Cl sensitivity to AoA. [23], [24] explain that drag rises significantly beyond stall angle due to flow separation and turbulence, mirrored in the current results. [25] and [16] noted that shock waves in supersonic regimes intensify drag and limit lift efficiency, especially at high AoA. The presence of vortex-induced asymmetry and separation zones at higher AoA values is consistent with [26]. The wake structures and unsteady flow fields at 10° AoA highlight the sensitivity of aerodynamic performance to AoA adjustments in slender fin configurations. From a design perspective, increasing AoA improves lift but introduces aerodynamic penalties such as higher drag and potential instabilities, suggesting the optimal AoA is below 10° to maximize lift-to-drag ratio and maintain flow stability. These findings substantiate the predictive accuracy of the k-ω SST turbulence model, validated by [27] and [28], consistent with the CFD study by [25].

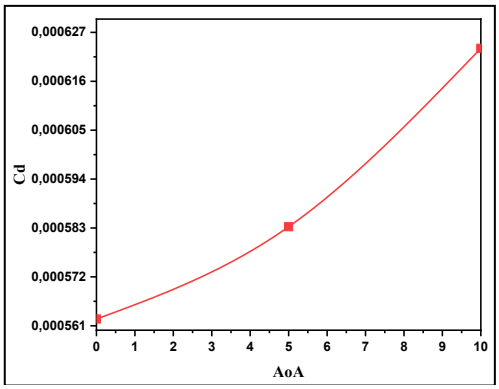


Figure 6. Variation of Cd at Different AoA

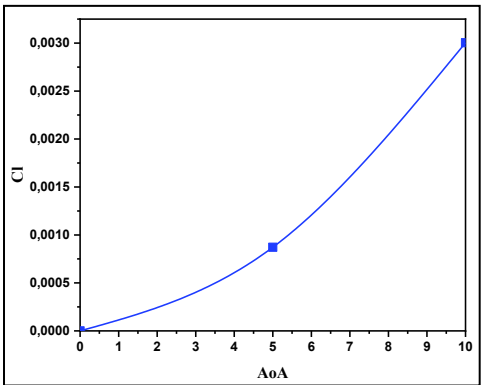


Figure 7. Variation of Cl at Different AoA

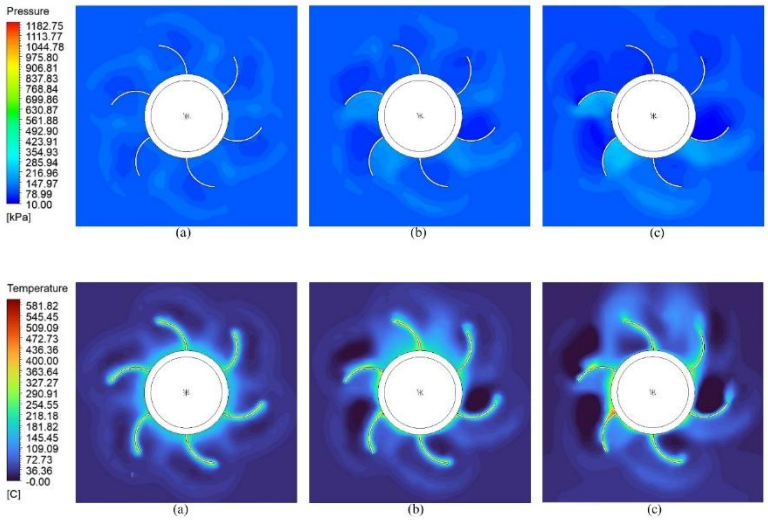


Figure 8. Contour Plots of Pressure and Temperature Distributions at Varying AoA, (a) = 0º, (b) = 5º, And (c) = 10º

Table 2. Aerodynamic Coefficients vs. AoA

AoA (º)	Cd	Cl	Cl/Cd Ratio
0	0.000562517	0.000000373	0.000663
5	0.000583283	0.000871799	1.494353
10	0.000623426	0.003003560	4.816773

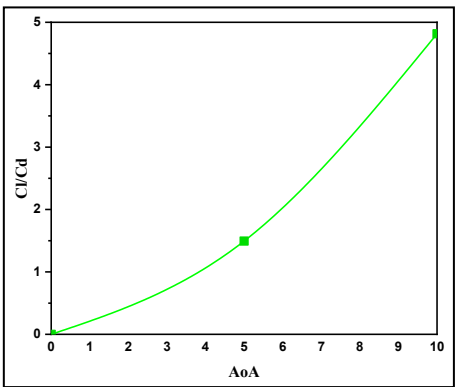


Figure 9. Cl/Cd Ratio as a Function of AoA

AIJASET – Vol. 05, No. 02, July 2025. 210-221
https://doi.org/10.25077/aijaset.v5i02.243

3.2 Influence of Fin Aspect Ratio

The simulation results indicate a strong correlation between the fin aspect ratio (a/b) and aerodynamic performance parameters, particularly the Cl and Cd. As depicted in Figure. 10, configurations with aspect ratios of 0.3, 0.5, and 0.8 demonstrate progressive changes in aerodynamic behavior under identical flow conditions. However, contrary to initial expectations, the Cl is observed to decrease with increasing aspect ratios. Specifically, fins with a/b = 0.3 yield the highest Cl value (approximately 0.00087), which gradually decreases to about 0.00063 at a/b = 0.8. This trend suggests that the lower aspect ratio configurations promote stronger lift performance, potentially due to enhanced localized flow attachment and minimized flow separation. In contrast, Figure. 11 presents the Cd values across the same aspect ratios. The results indicate a slight increase in Cd from about 0.000583 at a/b = 0.3 to approximately 0.000587 at a/b = 0.8, attributed to stronger shock interactions and larger wetted surface area at higher aspect ratios. Contour plots of pressure and temperature distributions (Figure. 12) corroborate these findings, showing more prominent high-pressure zones and complex thermal patterns as aspect ratio increases.

These results align with the studies of [29] and [13], who emphasized that aspect ratio influences both lift and drag through a combination of boundary layer stability and shock interaction mechanisms. However, while previous literature such as [30] and [16] suggest that higher aspect ratios generally enhance lift, the present findings highlight the importance of flow conditions and geometry interactions, revealing that lower aspect ratios might be more beneficial under the specific supersonic conditions examined. This is further supported by [31], who observed that shock wave interactions become more pronounced with increasing aspect ratio, contributing to greater drag. The reduction in lift with increasing aspect ratio may also relate to less efficient pressure distribution and vortex behavior, as described by [32] and [33]. From a design perspective, these insights suggest that a moderate aspect ratio (around 0.5) may provide an optimal balance between lift generation and drag control, while higher aspect ratios could introduce performance penalties in supersonic applications. These findings also validate the predictive capability of the k-ω SST turbulence model in capturing complex aerodynamic phenomena in fin-stabilized configurations, in line with the comprehensive CFD studies by [34].

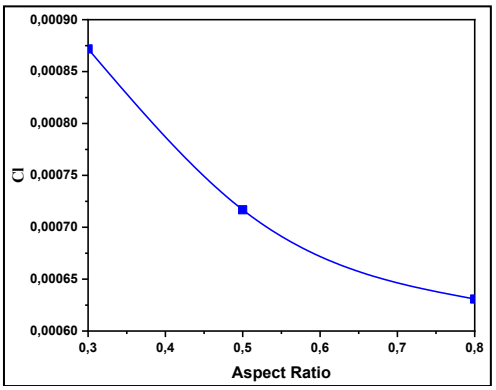


Figure 10. Variation of Aerodynamic Coefficients for Different Fin Aspect Ratios

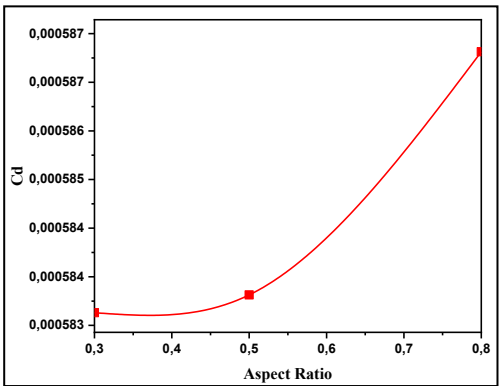


Figure 11. Cd Trends Across Different Fin Aspect Ratios

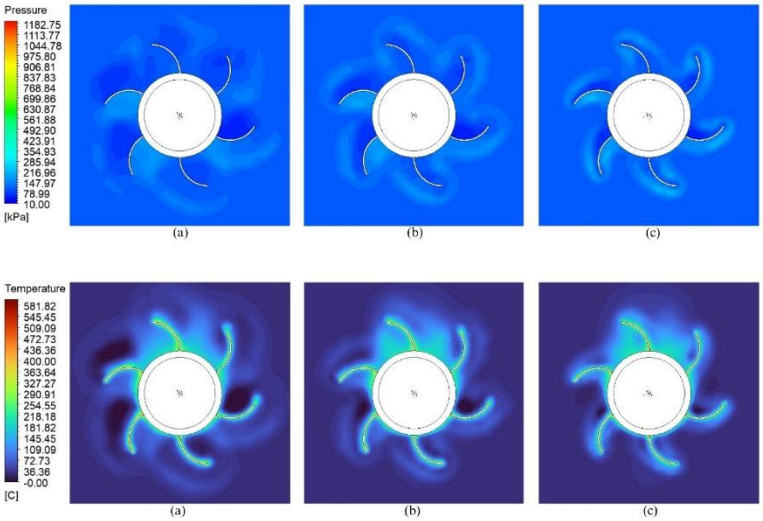


Figure 12. Pressure and Temperature Distribution Contours Illustrating Effects of Fin Aspect Ratio, (a) = 0.3, (b) = 0.5, and (c) = 0.8

Table 3. Aerodynamic Coefficients vs. Aspect Ratio

Fin Aspect ratio (a/b)	Cd	Cl	Cl/Cd Ratio
0.3	0.00058328297	0.00087179858	1.494584
0.5	0.00058353862	0.00071684995	1.228437
0.8	0.00058703934	0.00063079367	1.074728

3.3 Influence of Fin Radius of Curvature

The simulation results indicate that variations in the radius of curvature (R) at the fin leading edge substantially affect the aerodynamic characteristics of the rocket. As illustrated in Figure. 13 and Figure. 14, three radii of curvature (R = 20 mm, 30 mm, and 40 mm) were examined, revealing distinct patterns in the lift and drag coefficients. Specifically, the coefficient of lift (Cl) increases progressively with increasing radius of curvature, from approximately 0.000872 at R = 20 mm to around 0.000940 at R = 40 mm. Conversely, the Cd decreases with larger R, from approximately 0.000584 at R = 20 mm to about 0.000580 at R = 40 mm. These trends are corroborated by Figure. 15 and Table. 4, which depict the aerodynamic coefficients and lift-to-drag ratios for different R values. The pressure and temperature contours in Figure. 15 illustrate smoother pressure transitions and more uniform thermal distributions with increasing R, particularly at mid-chord sections. This indicates delayed shock formation and improved boundary layer stability, resulting in enhanced aerodynamic efficiency.

The observed aerodynamic behavior aligns with previous research. [35] demonstrated that blunt leading edges (larger R) generate weaker shock waves, reducing drag compared to sharper profiles. This supports the present findings where R = 40 mm shows better drag performance than R = 20 mm. Similarly, [36] highlighted that moderate curvature promotes smoother supersonic flow transitions and minimizes drag-inducing shock interactions. Boundary layer considerations, as discussed by [37], suggest that larger curvature enhances flow attachment and stability, which is supported by the current results showing greater lift at R = 30 mm and 40 mm. The presence of leading-edge vortices (LEVs) observed in the simulations, particularly at R = 30 mm and 40 mm, corroborates the findings of [38] and [39], who associated optimal vortex behavior with rounded geometries. From a design perspective, the results imply that adopting a radius of curvature around 30–40 mm can provide a balance between

aerodynamic performance and structural integrity. This balance is consistent with the optimization strategies outlined by [40], who used CFD and genetic algorithms to identify optimal curvature profiles. The findings validate the predictive accuracy of the k-ω SST turbulence model in capturing complex flow phenomena, as demonstrated by [41].

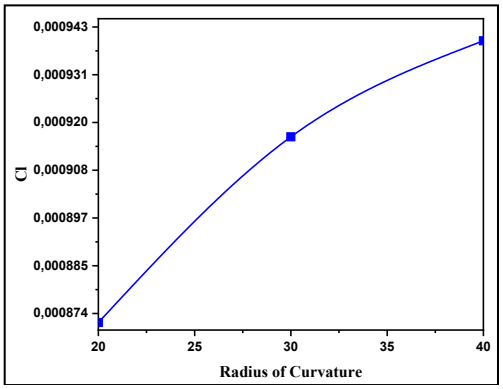


Figure 13. Aerodynamic Coefficient Variations for Different Radii of Curvature

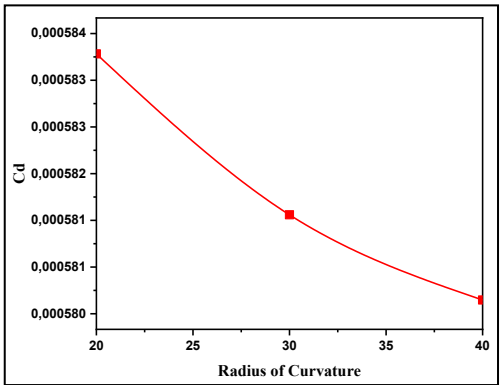


Figure 14. Cd Trends Across Different Radii of Curvature

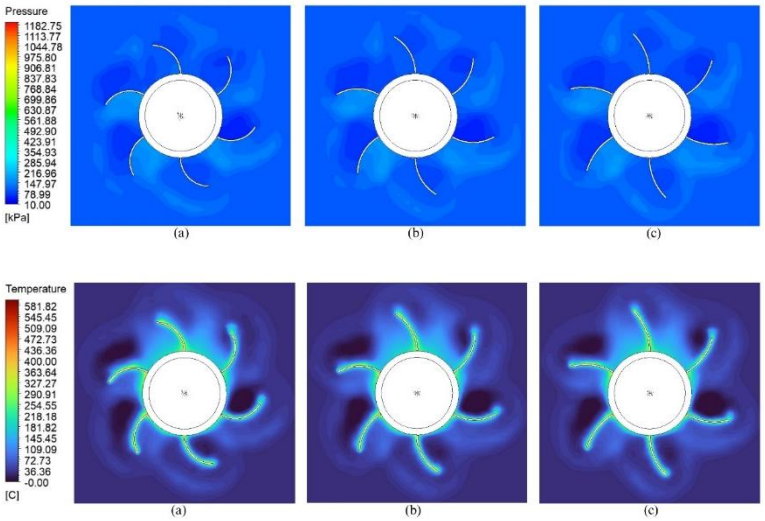


Figure 15. Contour Plots of Pressure and Temperature Distributions for Varying Radii of Curvature, (a) = 20 mm, (b) = 30 mm, and (c) = 40 mm

Table 4. Aerodynamic Coefficients vs. Fin Radius of Curvature

Radius of Curvature (mm)	Cd	Cl	Cl/Cd Ratio
20	0.000583539	0.000871799	1.494
30	0.000581472	0.000916532	1.576
40	0.000580377	0.000939663	1.619

4. Conclusion

This study investigated the aerodynamic behavior of a fin-stabilized rocket under supersonic flow by systematically varying the AoA, fin aspect ratio, and leading-edge radius of curvature using a full-factorial computational design approach. The results revealed that AoA significantly affects aerodynamic performance, with Cl increasing sharply and Cd rising moderately at higher AoA, indicating trade-offs between lift and drag. Optimal lift-to-drag ratios were achieved at moderate AoA values (below 10°) due to enhanced flow attachment and reduced separation. In contrast to prior

expectations, the findings indicate that lower aspect ratios (around 0.3) enhanced lift performance under the examined conditions, while higher aspect ratios increased drag due to shock interactions and flow complexity. Regarding leading-edge curvature, a progressive increase in R led to improved lift and reduced drag, with optimal performance observed around 30–40 mm due to smoother flow transitions and delayed shock formation. These results provide useful guidance for aerospace design practices, particularly in optimizing fin geometries to enhance aerodynamic efficiency in supersonic applications, such as missiles, space launch vehicles, and sounding rockets. Future research should expand on this work by incorporating unsteady flow effects, aeroelastic structural coupling, and thermal loading analysis, as well as validating the CFD results with wind tunnel experiments or flight test data to improve practical implementation and model reliability.

Acknowledgment

References

[1] C. Özel, C. K. Macit, and M. Özel, "Investigation of Flight Performance of Notched Delta Wing Rockets on Different Types of Nose Cones," *Turk. J. Sci. Technol.*, vol. 18, no. 2, pp. 435–447, 2023, doi: 10.55525/tjst.1245275.

[2] N. B. Jampi and M. F. Zulkafli, "The Effect of Moveable Fins on Trajectory and Aerodynamic Characteristics of Model Rockets," *Prog. Aerosp. Aviat. Technol.*, vol. 4, no. 1, 2024, doi: 10.30880/paat.2024.04.01.008.

[3] L. Sopegno, P. Livreri, M. Stefanovic, and K. P. Valavanis, "Thrust Vector Controller Comparison for a Finless Rocket," *Machines*, vol. 11, no. 3, p. 394, 2023, doi: 10.3390/machines11030394.

[4] A. Verhaegen and R. Żbikowski, "Aeroservoelastic Modelling and Control of a Slender Anti-Air Missile for Active Damping of Longitudinal Bending Vibrations," *Aerosp. Sci. Technol.*, vol. 66, pp. 20–27, 2017, doi: 10.1016/j.ast.2017.03.001.

[5] A. Andoko *et al.*, "Simulation of winglet with bend angles of 45, 60 and 90 degree," presented at the AIP Conference Proceedings, 2020. doi: 10.1063/5.0015757.

[6] Y. Chen, X. Gao, M. Gao, and H.-M. Lv, "Aerodynamic Characteristic of a Canard Guided Rocket," *Int. J. Model. Simul. Sci. Comput.*, vol. 08, no. 01, p. 1750001, 2017, doi: 10.1142/s1793962317500015.

[7] D. Santos, J. Rogers, A. d. Rezende, and V. Maldonado, "Exploring the Performance Boundaries of a Small Reconfigurable Multi-Mission UAV Through Multidisciplinary Analysis," *Aerospace*, vol. 10, no. 8, p. 684, 2023, doi: 10.3390/aerospace10080684.

[8] R. Ramadhan, A. Andoko, and S. Suprayitno, "Simulation of divergent angle of hybrid rocket engine nozzle using Ansys CFD," presented at the AIP Conference Proceedings, 2024. doi: 10.1063/5.0223224.

[9] D. Luo, "Numerical Simulation of Supersonic Turbulent Separated Flows Based on K–ω Turbulence Models With Different Compressibility Corrections," *Aerospace*, vol. 10, no. 12, p. 1014, 2023, doi: 10.3390/aerospace10121014.

[10] Z. Vasić, K. Maksimović, I. Vasović, M. Maksimović, and S. Maksimović, "Computational Fluid Dynamics and Strength Analysis of Composite UAV Wing," pp. 85–104, 2021, doi: 10.1007/978-3-030-86009-7_5.

[11] Md. H. M. Mazumder, "Comparative Study of Turbulence Models in CFD for Transonic Flow Over the ONERA M6 Wing," 2024, doi: 10.21203/rs.3.rs-4706004/v1.

[12] W. Zhang, M. Xia, and J. Zhu, "LPV Modeling and Identification of Unsteady Aerodynamics for Fast Maneuvering Aircrafts," *Ieee Access*, vol. 7, pp. 92436–92443, 2019, doi: 10.1109/access.2019.2927503.

[13] M. Tahani, M. Masdari, and M. Kazemi, "Aerodynamic Performance Improvement of a Canard Control Missile," *Aircr. Eng. Aerosp. Technol.*, vol. 89, no. 6, pp. 871–878, 2017, doi: 10.1108/aeat-01-2016-0019.

[14] A. Elshahomi *et al.*, "Computational Fluid Dynamics Performance Evaluation of Grooved Fins for Surfboards," *Mrs Adv.*, vol. 7, no. 30, pp. 695–700, 2022, doi: 10.1557/s43580-022-00311-5.

[15] H. Rao, Y. Shi, J. Bai, Y. Chen, T. Yang, and J. Li, "Aerodynamic Optimization Design of Supersonic Wing Based on Discrete Adjoint," *Aerospace*, vol. 10, no. 5, p. 420, 2023, doi: 10.3390/aerospace10050420.
[16] A. Şumnu, İ. H. Güzelbey, and O. Öğücü, "Aerodynamic Shape Optimization of a Missile Using a Multiobjective Genetic Algorithm," *Int. J. Aerosp. Eng.*, vol. 2020, pp. 1–17, 2020, doi: 10.1155/2020/1528435.
[17] D. S. Weaver and S. Mišković, "A Study of RANS Turbulence Models in Fully Turbulent Jets: A Perspective for CFD-DEM Simulations," *Fluids*, vol. 6, no. 8, p. 271, 2021, doi: 10.3390/fluids6080271.
[18] X. Zhang, M. Li, B. Wang, and Z. Li, "A Parameter Correction Method of CFD Based on the Approximate Bayesian Computation Technique," *J. Phys. Conf. Ser.*, vol. 2569, no. 1, p. 012076, 2023, doi: 10.1088/1742-6596/2569/1/012076.
[19] S. Evran and S. Z. Yildir, "Numerical and Statistical Aerodynamic Performance Analysis of NACA0009 and NACA4415 Airfoils," *J. Polytech.*, 2023, doi: 10.2339/politeknik.1229081.
[20] Y. A. Elawad and E. ElJack, "Numerical Investigation of the Low-Frequency Flow Oscillation Over a NACA-0012 Aerofoil at the Inception of Stall," *Int. J. Micro Air Veh.*, vol. 11, 2019, doi: 10.1177/1756829319833687.
[21] M. S. Arif *et al.*, "Laminar Flow Analysis of NACA 4412 Airfoil Through ANSYS Fluent," *Proc. Int. Exch. Innov. Conf. Eng. Sci. Ieices*, vol. 8, pp. 394–399, 2022, doi: 10.5109/5909123.
[22] Md. Zulkarna-En, Md. A. Islam, A. Al-Faruk, M. R. I. Pranto, and A. N. M. M. I. Mukut, "Numerical Analysis of Aerodynamic and Shock Wave Characteristics of Biconvex and Double-Wedge Shape Airfoils for Supersonic Flow," *Int. J. Automot. Mech. Eng.*, vol. 20, no. 4, pp. 10821–10837, 2023, doi: 10.15282/ijame.20.4.2023.02.0837.
[23] S. Eftekhari and A. S. M. Al-Obaidi, "Investigation of a NACA0012 Finite Wing Aerodynamics at Low Reynold's Numbers and 0º to 90º Angle of Attack," *J. Aerosp. Technol. Manag.*, 2019, doi: 10.5028/jatm.v11.1023.
[24] N. Nafroni, B. W. Riyandwita, and P. Adripta, "Effect of Variation of Angle of Attack on Lift and Drag Coefficient of Flat Plate Wing on Flying Inflatable Boat," 2023, doi: 10.4108/eai.23-11-2022.2341594.
[25] A. A. Gaonkar, P. Menon, and G. Srinivas, "Aerodynamic Performance Enhancement of Supersonic 2D Missile Using ANSYS," *Univers. J. Mech. Eng.*, vol. 7, no. 6A, pp. 1–11, 2019, doi: 10.13189/ujme.2019.071401.
[26] K. Kawauchi, T. Harada, K. Kitamura, and S. Nonaka, "Experimental and Numerical Investigations of Slender Body Side Force With Asymmetric Protuberances," *J. Spacecr. Rockets*, vol. 56, no. 5, pp. 1346–1357, 2019, doi: 10.2514/1.a34439.
[27] Q. Bourny, A. Proença, D. D. Pasquale, and S. Prince, "Analysis of Triangular Cross-Section Slender Bodies in Supersonic Regime Using RANS Simulations," 2023, doi: 10.2514/6.2023-4404.
[28] S. Saha, P. K. Sinha, and D. Chakraborty, "CFD Prediction of Ramjet Intake Characteristics at Angle of Attack," *Joast*, pp. 159–165, 2023, doi: 10.61653/joast.v62i3.2010.499.
[29] A. K. Bagheri, M. Pasandidehfard, and S. A. T. Sabour, "Numerical Investigation of Aerodynamic Effects of Opposite Wrap-Around Fins at Supersonic Speeds," *Proc. Inst. Mech. Eng. Part C J. Mech. Eng. Sci.*, vol. 233, no. 7, pp. 2410–2425, 2018, doi: 10.1177/0954406218784317.
[30] S. Khan, S. Malik, M. Junaid, and A. T. Jafry, "To Investigate and Compare the Wing Planform's Effect on the Aerodynamic Parameters of Aircraft Wings Using Computational Fluid Dynamics (CFD)," 2022, doi: 10.21203/rs.3.rs-1806010/v1.
[31] A. Coschignano, N. R. Atkins, H. Babinsky, and J. Serna, "Effect of Reynolds Number on a Normal Shock Wave-Transitional Boundary-Layer Interaction Over a Curved Surface," *Exp. Fluids*, vol. 60, no. 12, 2019, doi: 10.1007/s00348-019-2824-0.
[32] N. Nivedita, P. M. Ligrani, and I. Papautsky, "Dean Flow Dynamics in Low-Aspect Ratio Spiral Microchannels," *Sci. Rep.*, vol. 7, no. 1, 2017, doi: 10.1038/srep44072.

[33] M. H. W. Khin and S. Obi, "Numerical Study on the Hydrodynamic Performance of a Flexible Caudal Fin With Different Trailing-Edge Shapes," *Biomimetics*, vol. 9, no. 7, p. 445, 2024, doi: 10.3390/biomimetics9070445.
[34] A. Aşkan and S. Tangöz, "The Impact of Aspect Ratio on Aerodynamic Performance and Flow Separation Behavior of a Model Wing Composed From Different Profiles," *J. Energy Syst.*, vol. 2, no. 4, pp. 224–237, 2018, doi: 10.30521/jes.454215.
[35] L. Guo and S. Fang, "Study on Heat Reduction and Lift-to-Drag Ratio Increase of Two-Dimensional Wedge-Shaped Waverider Blunt Leading Edges and High Pressure Capture Wing[1] Combined Configuration," *J. Phys. Conf. Ser.*, vol. 2383, no. 1, p. 012127, 2022, doi: 10.1088/1742-6596/2383/1/012127.
[36] D. Bhatia, D. K. Yadav, G. Yang, J. Wang, and H. Hesse, "Selection and Impact of an Aerofoil Leading Edge on Boundary Layer Transition," *J. Transp. Technol.*, vol. 12, no. 04, pp. 778–803, 2022, doi: 10.4236/jtts.2022.124044.
[37] W. Zheng, "Numerical Simulation of the Airflow Near the Leading Edge and Trailing Edge of a Flat Plate," p. 71, 2022, doi: 10.1117/12.2655020.
[38] Q. Zhong, H. Dong, and D. Quinn, "How Dorsal Fin Sharpness Affects Swimming Speed and Economy," *J. Fluid Mech.*, vol. 878, pp. 370–385, 2019, doi: 10.1017/jfm.2019.612.
[39] D. Shormann, M. i. h. Panhuis, and L. Oggiano, "Field Research and Numerical CFD Analysis of Humpback Whale-Inspired Shortboard Fins," p. 158, 2020, doi: 10.3390/proceedings2020049158.
[40] K. Sakellariou, Z. A. Rana, and K. W. Jenkins, "Optimisation of the Surfboard Fin Shape Using Computational Fluid Dynamics and Genetic Algorithms," *Proc. Inst. Mech. Eng. Part P J. Sports Eng. Technol.*, vol. 231, no. 4, pp. 344–354, 2017, doi: 10.1177/1754337117704538.
[41] S. Puckett and V. Narayanaswamy, "High-Bandwidth Pressure Field Imaging of Fin-Generated Shock Wave–boundary Layer Interactions," *J. Fluid Mech.*, vol. 999, 2024, doi: 10.1017/jfm.2024.966.